Hindawi
Advances in Materials Science and Engineering
Volume 2019, Article ID 3790167, 15 pages
https://doi.org/10.1155/2019/3790167

Research Article

Thermosetting Coupling Analysis and Parameter Optimization of the Plastic Lining Pump Structure

Lingfeng Tang, Mingwei Liu, and Feihong Ma

School of Mechanical and Automotive Engineering, Anhui Polytechnic University, Wuhu, Anhui 241000, China

Correspondence should be addressed to Mingwei Liu; 1244084325@qq.com

Received 7 November 2018; Accepted 23 January 2019; Published 11 March 2019

Academic Editor: Alain Portavoce

In order to obtain the optimum structure of the lining pump under the condition of fluid thermosetting coupling, according to the given design parameters, the structural parameters of the pump were calculated, the three-dimensional geometric model was established, and the flow field analysis was carried out by CFD; the inlet angle β_{b1}, outlet angle β_{b2}, wrap angle φ, inlet diameter D_1, and outlet diameter D_2 of the impeller were selected as the five factors to design orthogonal experiment, and the results were analyzed by range analysis; then, the efficiency and cavitation allowance were obtained as combined parameters under the evaluation index. The displacement deformation and stress distribution under the condition of the coupling field were obtained by the fluid-solid coupling analysis, and the orthogonal experimental table of the impeller structure of the lining plastic pump was established, and then the orthogonal experimental results are analyzed to obtain the influence of each structural parameter under the condition of each evaluation index and the optimum combination parameters. The influence situation and the best combination parameters under the condition of evaluation index, taking the minimum displacement deformation and minimum stress of impeller as the reference index, and the optimum combination parameters under the condition of minimum displacement and stress were as follows: the inlet diameter D_1 was 76 mm, the outlet diameter D_2 was 252 mm, the inlet angle was 26°, the outlet angle was 24°, and the wrap angle was 115°. Finally, the 3D printing technology was used to print out the physical model to the hydraulic performance experiment verification.

1. Introduction

Pumps are widely used and undertake a very important position in the fields such as agriculture and industry. In recent years, with the development of nonferrous metallurgy, the requirements for centrifugal pumps are growing higher [1]. Compared with metal pumps, the lining plastic pump has been widely used for their excellent corrosion resistance; therefore, the study on the lining plastic pump is increasingly important [2, 3]. In the process of conveying medium, the fluid in the pump interacts with the impeller [4, 5]; the lining plastic pump generates thermal stress in the process of pumping hot medium, which causes thermal deformation and the clearance between the impeller and the front pump cover changes [6, 7]. If the clearance is too small, the liquid will cause expansion and deformation of the pump shell; in addition, it will generate friction between the impeller and the front pump cover and aggravates the wear of the impeller due to heat; relatively, if the clearance is too large, there will be backflow between the pump shell and the impeller, thus reducing the volumetric efficiency. At present, when most scholars at home and abroad conducting research [8, 9], the conduction of CFD internal flow field analysis and fluid-thermal-structure interaction on the plastic lined pump has been neglected [10, 11]. In this paper, using CFD to analyze the flow field of the lining plastic pump, through orthogonal experiment and range analysis, it could be concluded that the efficiency and cavitation allowance were taken as the combined parameters under the evaluation index. Taking the minimum displacement deformation and minimum stress of impeller as the reference index, the combined weighted scoring method and Taguchi algorithm were used to optimize the parameters of the thermal-solid coupling analysis of the

lining plastic pump flow, and the optimum combination parameters under the condition of minimum displacement and stress were obtained.

2. Structure Design

The basic parameters of the lining plastic pump are as follows: flow rate $Q = 25^{\circ}\text{m}^3/\text{h}$, head $H = 80$ m, rotate speed $n = 2900$ rpm, inlet diameter of impeller $D_1 = 75$ mm, outlet diameter $D_2 = 255$ mm, width of impeller inlet $b_1 = 20$ mm, outlet width $b_2 = 7$ mm, impeller inlet angle is 25°, outlet angle is 30°, and the wrap angle is 110°. The physical model of impeller and volute-type discharge passage is established and assembled according to the above parameters, which is shown in Figure 1.

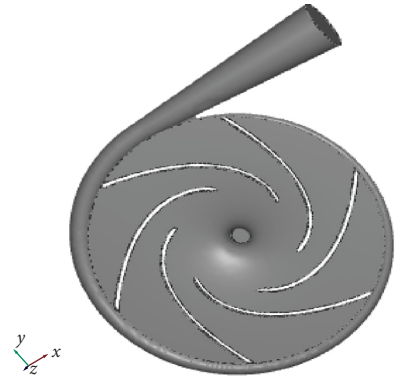

Figure 1: Fluid domain model.

3. Meshing and Flow Field Simulation

3.1. Meshing. Meshing is the basis of numerical discretization of flow control equations, and the quality of meshing directly influences the convergence of analysis and the accuracy of results. The grid number of the impeller region was 127,794, the volute region 727,398, and the inlet section 2408, a total of 854,692, as shown in Figure 2. The mesh is unstructured, 3D type, the minimum mesh was 0.0001, and the maximum is 0.025.

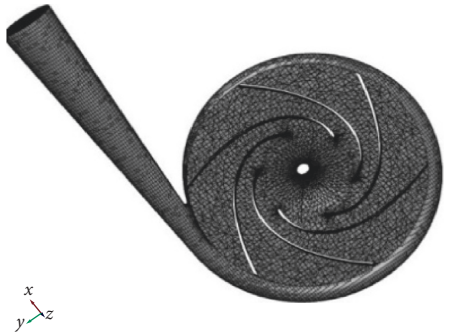

Figure 2: Mesh generation.

3.2. Boundary Conditions. The boundary conditions were mainly set as follows: the basic properties of the fluid medium, including the density, temperature, viscosity, vapor density, gas content, saturated vapor pressure, etc. as shown in Table 1. In addition to the rotor setting of the impeller blade, the setting of the inlet and outlet of the fluid medium and the setting of the rotating surface were also required.

The pressure here was the standard atmospheric pressure, set to the inlet condition, the flow rate, $Q = 25^{\circ}\text{m}^3/\text{h}$, was set to the export condition, the blade as a rotating part was set to a rotating speed of 2900 rpm, and the rest surface could be directly acquiesced to the static surface.

Table 1: Boundary condition setting.

Name of parameter	Parameter values
Fluid medium	Water
Density	998 kg/m^3
Reference temperature	300 K
Vapour density	0.0245 kg/m^3
Gas content	2.3×10^{-5}
Saturated vapor pressure	3610 pa
Bulk modulus	2.15×10^9

3.3. Control Equations. The flow of medium in plastic-lined pump satisfies the following equation:

Continuity equation:

$$\frac{\partial(\rho\mu_i)}{\partial x_i} = 0. \tag{1}$$

Momentum equation:

$$\frac{\partial(\rho\mu_i\mu_j)}{\partial x_j} = -\frac{\partial p^*}{\partial x_j} + \frac{\partial\left[\mu\left(\left(\partial x_j/\partial\mu_i\right) + \left(\partial\mu_j/\partial x_i\right)\right)\right]}{\partial x_j} - 2\varepsilon_{ijk}k\omega_j\mu_k. \tag{2}$$

Incompressible N-S equation:

$$\frac{\partial U_i}{\partial t} + U_j\frac{\partial U_i}{\partial x_j} = f_i - \left(\frac{1}{\rho}\frac{\partial p^*}{\partial x}\right)_i + \vartheta\nabla^2 U_i. \tag{3}$$

k-ε equation:

$$\rho\frac{dk}{dt} = \frac{\partial}{\partial x_j}\left[\left(\mu + \frac{\mu_t}{\sigma_k}\right)\frac{\partial k}{\partial x_j}\right] + G_k - \rho\varepsilon,$$

$$\rho\frac{d\varepsilon}{dt} = \frac{\partial}{\partial x_i}\left[\left(\mu + \frac{\mu_t}{\sigma_\varepsilon}\right)\frac{\partial k}{\partial x_i}\right] + \rho\varepsilon C_1 E - \rho C_2\frac{\varepsilon^2}{k + \sqrt{\vartheta\varepsilon}}, \tag{4}$$

$$\mu_t = \rho C_\mu\frac{k^2}{\varepsilon},$$

where ρ is the fluid density; ρ^* is the pressure including centrifugal force and turbulent kinetic energy k; ω is the angular velocity; ε_{ijk} is the tensor; μ is the effective viscosity coefficient; U is the velocity vector; P is the pressure; t is the time; ϑ is the viscosity coefficient of fluid motion; i, j, and k, respectively, are 1, 2, and 3; $\sigma_k = 1.0$; $\sigma_\varepsilon = 1.3$; $C_\mu = 0.09$; $C_1 = 1.44$; $C_2 = 1.92$.

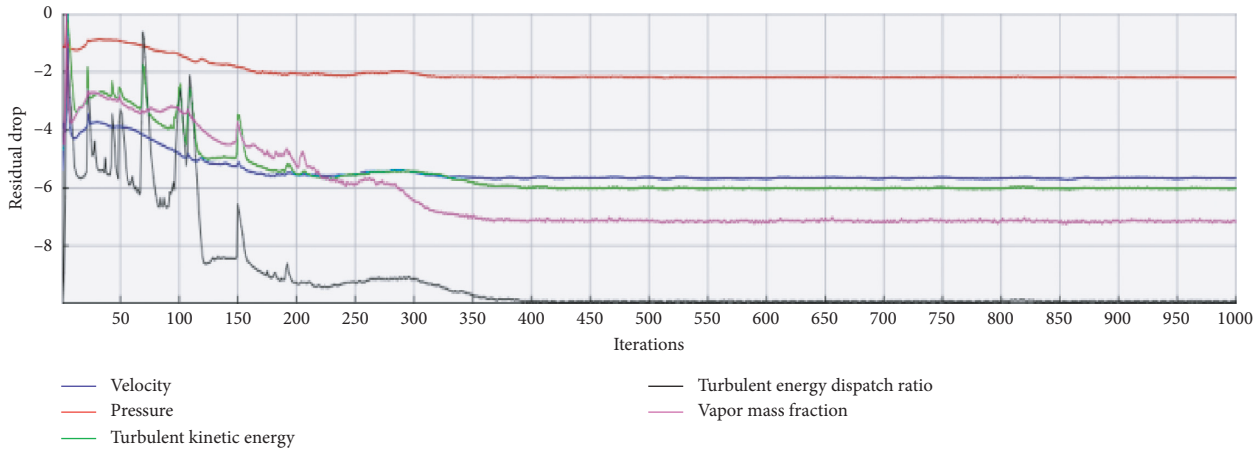

Figure 3: Residual curve.

3.4. Flow Field Simulation. There are 1,000 iteration steps for the lining plastic pump, and it can be seen from Figure 3 that the curve converged when the number of iterations reached about 500 times.

Figure 4 shows the pressure distribution of the lining plastic pump, from the inlet of the impeller to its outlet; the pressure value was increasing, and the value near the outlet of the volute was higher than elsewhere, mainly because the flow of the fluid is accompanied by the rotation of the impeller during the conveying process, and the inhomogeneity of its flow made it possible for vortices to appear between the adjacent.

Figure 5 is a speed distribution diagram of the lining plastic pump. As can be observed from Figure 5, the value of velocity was gradually increased from the entrance of the impeller to its outlet. The flow of liquid away from the blades was much less effective than the flow of the liquid at its periphery due to the action of the blades, and there would be swirl along the radial direction away from the middle of the blade, affecting the normal flow of the liquid.

According to the overall pressure distribution diagram in Figure 6, there is a low pressure area appearing in the impeller of the lining plastic pump, and negative pressure area on the back side of the blade working close to the volute tongue, where cavitation occurs easily.

As can be seen from Figure 7, due to the low pressure at the impeller inlet, the medium vaporization at room temperature reached the critical pressure, so cavitation occurred at the inlet of the impeller; the gas volume fraction was 0.84836, which was consistent with the actual situation.

4. Orthogonal Experiment and Range Analysis

4.1. Orthogonal Experiment. In the orthogonal experiment of the lining plastic pump, the interaction among the experimental factors was not yet considered. Taking the efficiency and cavitation erosion of the lining plastic pump into consideration, five structural dimensions of impeller inlet diameter, impeller outlet diameter, impeller inlet angle, outlet angle, and wrap angle were selected as experimental factors, and four levels were set for each factor, as shown in Table 2.

For the orthogonal experiment with four levels of five factors, the orthogonal table that could selected is L_{16} (4^5). Orthogonal experiment of lining pump is shown in Table 3.

4.2. Range Analyses. By means of mathematical statistics, the effects of each factor level on the efficiency and cavitation of the lining plastic pump and the combination parameters under the conditions of each evaluation index were analyzed. The following is a convenient description of the range analysis results. A, B, C, D, and E are, respectively, used to represent the inlet diameter of impeller D_1, outlet diameter D_2, inlet angle β_{b1}, outlet angle β_{b2}, and inclusion wrap angle φ.

4.2.1. Analysis of the Influence Trend of Various Factors on Efficiency. Table 4 shows that the influence degree of various factors on efficiency is from high to low, respectively, impeller outlet diameter D_2, wrap angle φ, impeller inlet diameter D_1, impeller inlet angle β_{b1}, and impeller exit angle β_{b2}. In order to observe the change trend more intuitively, the influence of various factors on efficiency was drawn, as shown in Figure 8. According to the evaluation indexes, the optimal level combination was $A_2B_4C_4D_1E_2$, that is, when the inlet diameter D_1 was 74 mm, outlet diameter D_2 was 258 mm, inlet angle was 20°, outlet angle was 30°, and wrap angle was 105°, and a the minimum loss could be obtained, which indicated the maximum efficiency of the lining plastic pump under this parameter. The optimized structure parameters of the lining plastic pump were not included in the existing tests. The CFD software was used to conduct the experimental verification again, and the maximum efficiency of the data is 56.80%, which was found to be close to the maximum value in the orthogonal experiment by comparison with the 16 experimental data.

4.2.2. Analysis of Influence Trend of Various Factors on Cavitation Erosion. It could be clearly seen from Table 5 that the influence of various factors on cavitation was, respectively, inlet angle β_{b1}, wrap angle φ, outlet diameter of impeller D_2, outlet angle β_{b2}, and inlet diameter D_1. In order to observe the change trend more intuitively, the influence of

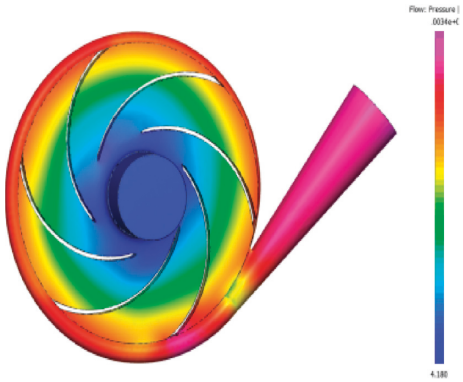

Figure 4: Pressure cloud diagram.

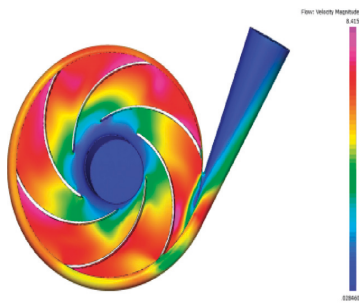

Figure 5: Velocity cloud.

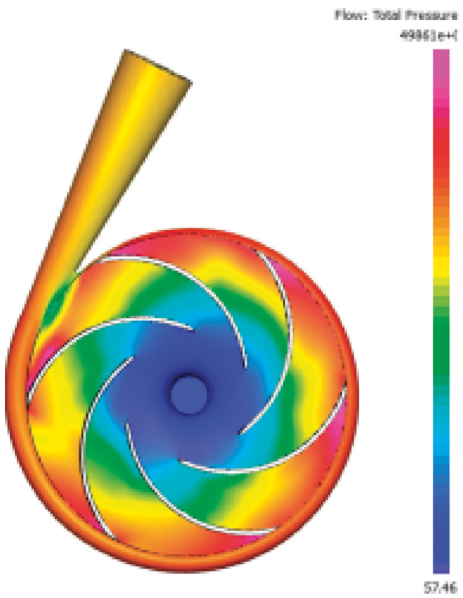

Figure 6: Overall pressure distribution.

various factors on the gas volume fraction was plotted, as shown in Figure 9. According to the evaluation indexes, the optimal level combination for $A_2B_2C_1D_3E_1$, that is, the inlet diameter D_1 was 74 mm, outlet diameter D_2 was 254 mm, the inlet angle was 18°, the outlet angle was 28°, and the wrap angle was 100°, while the gas volume fraction of the lining plastic pump was minimum, showed that the cavitation of the lining pump had a better improvement. The optimized

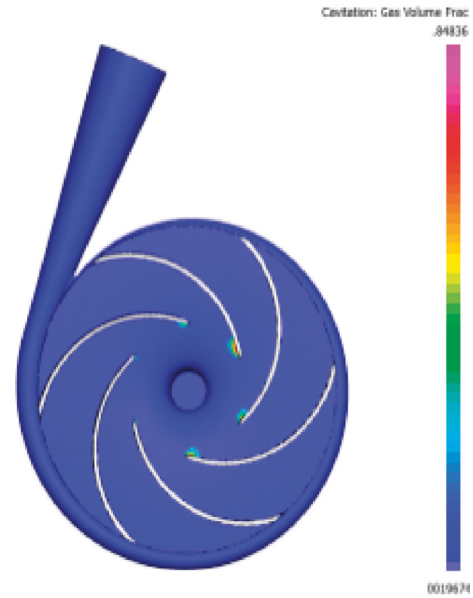

Figure 7: Gas volume fraction diagram.

structure parameters of the lining plastic pump were not included in the existing tests. The CFD software was used to remodel and verify the test results, and the minimum gas volume fraction obtained of this group was 0.84346.

4.3. Influence of Enveloping Angle on Pump Performance. The angle between the connection of the inlet edge and the center of the blade, and the connection of the outlet side and the center of the circle is called the blade packet angle. The wrap angle directly affected the length of the flow passage between the two blades. The longer the flow passage between the two blades is, the larger the wrap angle would be, and the smaller the unit load on the blade per unit length would be. Meanwhile, the smaller the diffusion degree of the flow passage is, the stronger the control ability of the flow passage on the liquid would be, and the energy could be effectively transferred.

However, when the blade wrap angle was too large, the increase of the distance from the impeller inlet to the outlet of the liquid resulted in the increase of the friction loss between the blade and the liquid, which is not only conducive to the energy exchange but also caused loss of most of the head. In addition, due to the difference of casting technology level, too much wrapping angle would also be limited by the technology level, so the size of wrapping angle should be selected appropriately. It is well known that when the specific speed of the pump is between 60 and 120, wrap angle will usually be $\varphi = 75°–150°$, then the specific speed will change from low to high, and finally the blade wrap angle value changes from large to small. However, in the actual drawing process, the wrap angle should be adjusted according to the specific situation. As an important geometric parameter of the blade, on the premise of the projection diagram of the axial plane of the blade and the number of blades, the wrap angle essentially reflects the diffusion degree of the blade passage. As the blade wrap

Table 2: Orthogonal experimental factors of lining pump impeller level.

	Inlet diameter D_1 (mm)	Outlet diameter D_2 (mm)	Inlet angle β_{b1} (°)	Outlet angle β_{b2} (°)	Wrap angle φ (°)
1	72	252	18	20	100
2	74	254	22	24	105
3	76	256	26	28	110
4	78	258	30	32	115

Table 3: Orthogonal experimental results of impeller structure.

Experiment number	Import diameter D_1 (mm)	Exit diameter D_2 (mm)	Import angle β_{b1} (°)	Exit angle β_{b2} (°)	Wrap angle φ (°)	Efficiency η (%)	Gas volume fraction
1	72	252	18	20	100	57.13	0.848360
2	72	254	22	24	105	52.53	0.874810
3	72	256	26	28	110	53.45	0.867331
4	72	258	30	32	115	57.45	0.874301
5	74	252	22	28	115	57.80	0.880091
6	74	254	18	32	110	53.86	0.823669
7	74	256	30	20	105	57.99	0.819132
8	74	258	26	24	100	57.76	0.873608
9	76	252	26	32	105	59.39	0.828129
10	76	254	18	28	100	54.47	0.867710
11	76	256	30	24	115	55.46	0.871944
12	76	258	22	20	110	57.29	0.944049
13	78	252	30	24	110	56.88	0.882889
14	78	254	26	20	115	55.26	0.906458
15	78	256	22	32	100	53.60	0.838161
16	78	258	18	28	105	59.01	0.845031

Table 4: Influence data of various factors on efficiency.

	D_1	D_2	β_{b1}	β_{b2}	φ
K1	220.56	231.2	224.47	227.67	222.96
K2	227.41	216.12	221.22	222.63	228.92
K3	226.61	220.5	225.86	224.73	221.48
K4	224.75	231.51	227.78	224.24	225.97
$\overline{K1}$	55.14	57.8	56.1175	56.9175	55.74
$\overline{K2}$	56.85	54.03	55.305	55.6575	57.23
$\overline{K3}$	56.65	55.125	56.465	56.1825	55.37
$\overline{K4}$	56.1875	57.8775	56.945	56.06	56.4925
Range	1.71	3.8475	1.64	1.26	1.86
Sequencing	3	1	4	5	2

angle increases, the flow head curve drops more and more steeply while the flow powers curve flatten out. According to experience, the wrap angle generally takes 90° to 130°.

Figure 10 indicates blade wrap angles of 95°, 100°, 105°, 110°, and 115° of 5 kinds of centrifugal pump in the outlet flow show lift efficiency curves under 0.8 Q_d, 0.9 Q_d, 0.96 Q_d, 1.0 Q_d, 1.1 Q_d, and 1.2 Q_d conditions.

From Figure 10, the following observations are made:

(1) The influence of blade wrap angle on the lift of centrifugal pump with high ratio speed was greater than that of efficiency; the smaller the wrap angle is, the larger the lift of the centrifugal pump would be, and the more the trend of decreasing tends to fit straight line.

(2) At low flow rate, the smaller the wrap angle is, the lower the efficiency of the centrifugal pump would be; in large flow, the larger the wrap angle, the lower the efficiency of the centrifugal pump, and the faster the decline, the most obvious when the wrap angle, which was 115.

(3) In 0.96 Q_d centrifugal pump, to achieve the highest efficiency point, when the blade angle was 110°, the efficiency was superior to the other angle of the impeller. This is because, with the increase in the wrap angle, the blade became longer, the blade's restraint on the fluid in the flow passage increased, and the efficiency increased. However, when the wrap angle was too large, the friction on the fluid increased, and the maximum efficiency dropped. There was an optimal blade wrap angle to make the centrifugal pump to have the best efficiency.

4.4. Multifield Coupling Analysis of Liner Pump Structure. By analyzing the flow thermal and solid coupling of the impeller structure of the lining plastic pump, the displacement distribution cloud map and stress distribution cloud map can be obtained, as shown in Figures 11 and 12, respectively. It can be seen from Figure 11 that the deformation distribution showed a gradual increasing trend along the central axis of the impeller structure, and the maximum deformation was close to the edge of the impeller, the maximum deformation along the radial direction of the impeller was 1.7717 mm, and the minimum deformation was located at its central axis. This was mainly due to the fixed constraint at the central shaft and free expansion and deformation end at the edge of the impeller when the thermo-solid coupling analysis of the liner pump impeller structure was carried out.

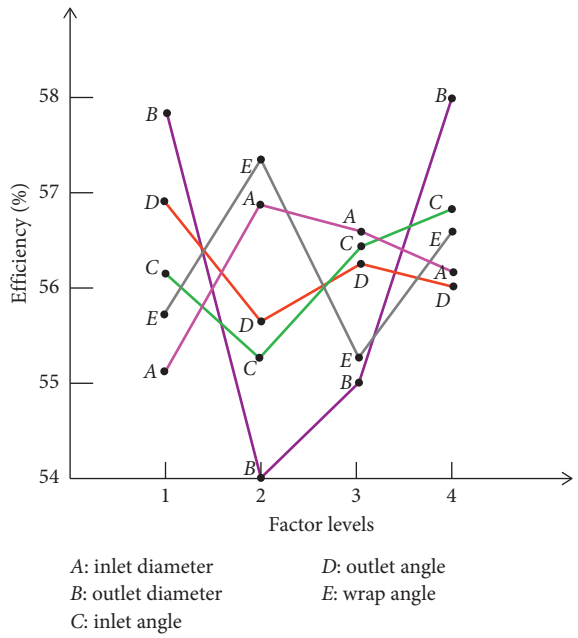

Figure 8: Influence trend of each parameter on efficiency.

Table 5: Influence data of various factors on cavitation.

	D_1	D_2	β_{b1}	β_{b2}	φ
K1	3.464802	3.439469	3.28477	3.517999	3.327839
K2	3.3965	3.372647	3.53711	3.503251	3.367102
K3	3.411832	3.396568	3.475526	3.360163	3.517938
K4	3.472539	3.536989	3.448266	3.36426	3.532794
$\overline{K1}$	0.86620	0.859867	0.821190	0.87950	0.831960
$\overline{K2}$	0.849125	0.843162	0.884278	0.875813	0.841776
$\overline{K3}$	0.82958	0.849142	0.86888	0.840041	0.879485
$\overline{K4}$	0.868135	0.884247	0.8620665	0.841065	0.88320
Range	0.01901	0.041085	0.063088	0.039459	0.05124
Sequencing	5	3	1	4	2

Through observation and analysis of Figure 12, it can be seen that the maximum stress was mainly concentrated at the central axle hole, and the increase in radial dimension along the impeller shows a decreasing trend. The closer it was to the edge, the smaller the stress was, and the maximum equivalent stress was 10.31°Mpa. Stress comes mainly from two sources, on the one hand, when the fluid pressure load was applied to the working face of the impeller, the working face of the impeller will bear large load pressure and generate stress deformation, and on the other hand, when temperature load was applied to the working face of the impeller, it will produce thermal deformation and thermal stress.

4.5. Orthogonal Table Design. Taking the total displacement deformation and stress distribution of the lining plastic pump into comprehensive consideration, five parameters including inlet diameter of the impeller, outlet diameter of the impeller, inlet angle, outlet angle, and cladding angle of the impeller were selected as experimental factors, and four levels were set for each factor. The orthogonal experimental factors of the liner plastic pump are shown in Table 6.

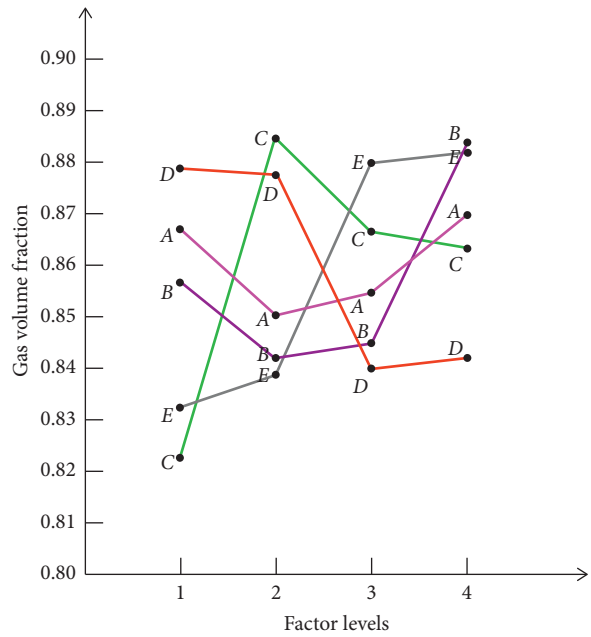

Figure 9: Influence trend of each parameter on gas volume fraction.

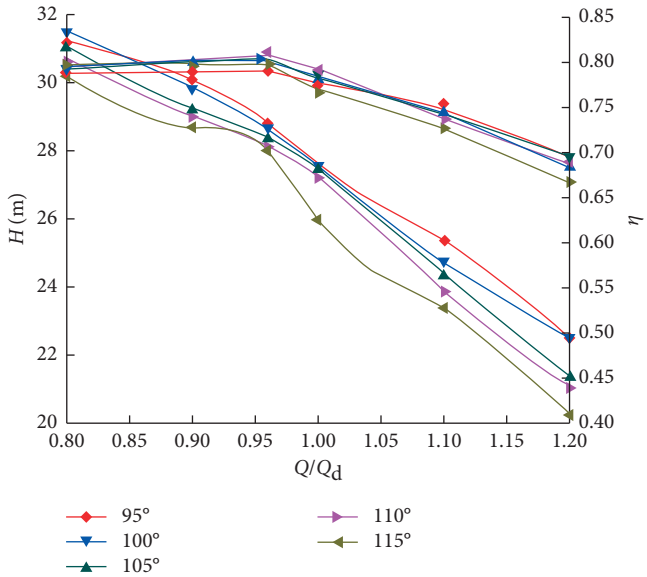

Figure 10: Centrifugal pump head: efficiency curve.

4.6. Orthogonal Experimental Results and Range Analysis. By conducting orthogonal experiments on the lining plastic pump structure under fluid-thermal-structure interaction conditions, the orthogonal experimental table of the lining plastic pump structure under fluid-thermal-structure interaction conditions can be obtained as shown in Table 7. According to the orthogonal experimental results of the lining plastic pump structure in Table 8, the maximum

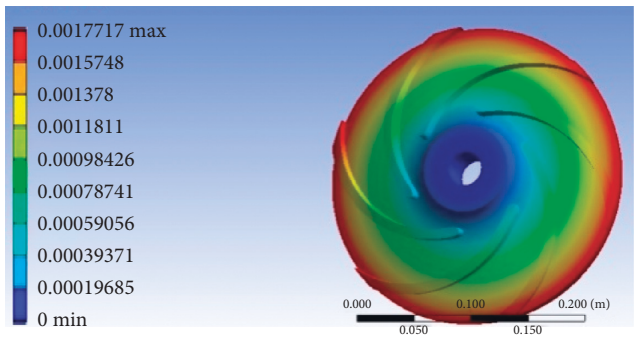

Figure 11: Total displacement deformation cloud map.

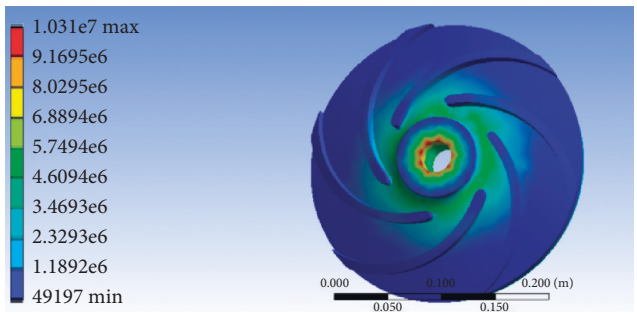

Figure 12: Cloud diagram of stress distribution.

Table 6: Orthogonal experimental factors of lining pump impeller level table.

	Import diameter D_1 (mm)	Exit diameter D_2 (mm)	Inlet angle β_{b1} (°)	Outlet angle β_{b2} (°)	Wrap angle φ (°)
1	72	252	18	20	100
2	74	254	22	24	105
3	76	256	26	28	110
4	78	258	30	32	115

difference analysis value of the average value of total displacement and stress of each factor at each level was calculated. The calculation results are shown in Table 8.

It can be clearly seen from Table 8 that the influence of various factors on the total displacement was from large to small, respectively, the outlet diameter D_2, wrap angle φ, outlet angle β_{b2}, the inlet diameter D_1, and the inlet angle β_{b1}. Figure 13 shows the influence trend of various factors on the total displacement. According to the evaluation index, the optimal level combination was $A_3B_1C_3D_4E_4$, that is, the inlet diameter D_1 was 76 mm, outlet diameter D_2 was 252 mm, the inlet angle was 26°, the outlet angle was 32°, the wrap angle was 115°, while the total displacement of the lining plastic pump was minimum, which means that the lining plastic pump under this parameter had the minimum deformation.

According to the orthogonal experiment results of lining plastic pump structure in Table 7, the maximum difference analysis value of the average stress distribution under each level of each factor was calculated. It can be clearly seen from Table 9 that the influence of various factors on the stress was, respectively, diameter D_1, the inlet angle β_{b1}, the outlet diameter D_2, wrap angle φ, and outlet angle β_{b2}. Figure 14 shows the influence trend of various factors on stress. According to the evaluation index, the optimal level combination was $A_3B_1C_3D_2E_2$, that is, the inlet diameter D_1 was 76 mm, outlet diameter D_2 was 252 mm, the inlet angle was 26°, the outlet angle was 24°, and the wrap angle was 105°, while the stress of the lining plastic pump was minimum, which showed that the lining plastic pump under this parameter has minimal stresses.

4.7. Taguchi Algorithms Used to Optimize the Structural Parameters of the Lining Plastic Pump. In this chapter, the comprehensive weighted scoring method was used to analyze the orthogonal experimental results in the previous chapter. The comprehensive weighting method was a mathematical statistical method which converted the multi-index experiment into a single index one. It was a method which used the total score of each experiment to represent the experimental results. In this paper, the relevant knowledge of mathematical statistics is used to analyze and process the test results, and the score value of the comprehensive weighted score is calculated [12, 13].

Y_j^* was used to represent the sum of weighted scores of each performance index, and the larger Y_j^* was, the better the comprehensive performance of this group of tests will be. The formula for calculating the comprehensive weighted scores is as follows:

$$Y_j^* = \sum_{i=1}^{2} [Y(i, j) \times \omega_i]. \quad (5)$$

4.8. Comprehensive Weighted Scoring Results of Plastic-Lined Pump Impeller Structure. The results of the 16 orthogonal experiments obtained in the previous chapter were calculated by comprehensive weighted scoring. The results are shown in Table 10; group 9 had the largest value and Y_j^* score was 98.8, The combined parameters were $A_3B_1C_3D_4E_2$, that is, the inlet diameter D_1 was 76 mm, the outlet diameter D_2 was 252 mm, the inlet angle was 26°, the outlet angle was 32°, and the wrap angle was 105°.

4.9. Formulating Controllable Factors and Their Level Tables. Taking the total displacement, deformation, and stress distribution of the plastic-lined pump into comprehensive consideration, five structural dimensions of impeller inlet diameter, impeller outlet diameter, impeller inlet angle, impeller outlet angle, and wrap angle were selected as experimental factors, and four levels were set for each factor. Table 11 shows the controllable factors and their levels, the inlet angle β_{b1}, outlet angle β_{b2}, wrap angle φ, inlet diameter D_1, and outlet diameter D_2 of the pump.

4.10. Taguchi Test Design. The internal table of the orthogonal experiment was L_{16} (4^5). As shown in Table 12, since the index of the subsequent Taguchi experiment was

Table 7: Orthogonal experimental table of flow thermal and solid coupling of pump.

Experiment number	D_1 (mm)	D_2 (mm)	β_{b1} (°)	β_{b2} (°)	φ (°)	Total displacement (m)	Stress (Pa)
1	72	252	18	20	100	0.0017717	1.0310e7
2	72	254	22	24	105	0.0018074	1.0465e7
3	72	256	26	28	110	0.0018029	1.0592e7
4	72	258	30	32	115	0.0018044	1.1021e7
5	74	252	22	28	115	0.0016985	1.0678e7
6	74	254	18	32	110	0.0017669	1.1259e7
7	74	256	30	20	105	0.0018015	1.0710e7
8	74	258	26	24	100	0.0018828	1.0302e7
9	76	252	26	32	105	0.0016658	9.4937e6
10	76	254	18	28	100	0.0017558	1.1164e7
11	76	256	30	24	115	0.0017937	1.0386e7
12	76	258	22	20	110	0.0018422	1.0687e7
13	78	252	30	24	110	0.0017371	1.1217e7
14	78	254	26	20	115	0.0017607	1.0982e7
15	78	256	22	32	100	0.0018231	1.1333e7
16	78	258	18	28	105	0.0018562	1.1055e7

Table 8: Influence data of various factors on total displacement.

	D_1	D_2	β_{b1}	β_{b2}	φ
K1	7.1864×10^{-2}	6.8731×10^{-2}	7.1506×10^{-2}	7.1761×10^{-2}	7.2334×10^{-2}
K2	7.1497×10^{-2}	7.0908×10^{-2}	7.1712×10^{-2}	7.221×10^{-2}	7.1309×10^{-2}
K3	7.0575×10^{-2}	7.2212×10^{-2}	7.1122×10^{-2}	7.1134×10^{-2}	7.1491×10^{-2}
K4	7.1771×10^{-2}	7.3856×10^{-2}	7.2088×10^{-2}	7.0602×10^{-2}	7.0573×10^{-2}
$\overline{K1}$	1.7966×10^{-2}	1.7183×10^{-2}	1.7877×10^{-2}	1.7940×10^{-2}	1.8084×10^{-2}
$\overline{K2}$	1.7874×10^{-2}	1.7727×10^{-2}	1.7928×10^{-2}	1.8053×10^{-2}	1.7827×10^{-2}
$\overline{K3}$	1.7644×10^{-2}	1.8053×10^{-2}	1.7781×10^{-2}	1.7784×10^{-2}	1.7873×10^{-2}
$\overline{K4}$	1.7943×10^{-2}	1.8464×10^{-2}	1.8022×10^{-2}	1.7651×10^{-2}	1.7643×10^{-2}
Range	0.0326×10^{-2}	0.1281×10^{-2}	0.0241×10^{-2}	0.0402×10^{-2}	0.0441×10^{-2}
Sequencing	4	1	5	3	2

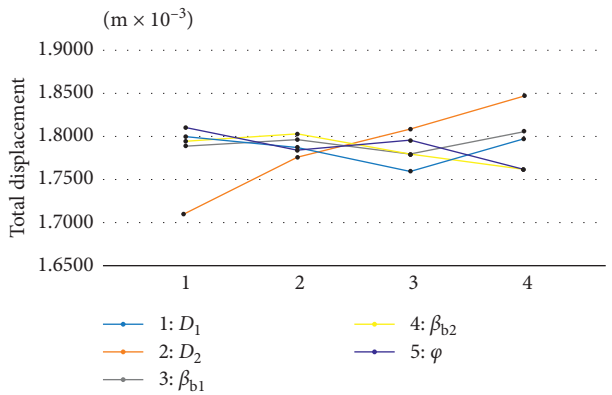

Figure 13: The influence trend of each parameter on the total displacement.

SN ratio rather than the quality characteristic, the interaction between factors was not considered [14–16].

4.10.1. Calculating the SN Ratio. In view of the fact that in practical applications, the displacement and stress are expected to be as small as possible. In taguchi algorithm, it is called the smaller-the-better characteristic Y_x and its SN ratio is calculated as follows [17]:

Table 9: Influence data of various factors on stress.

	D_1	D_2	β_{b1}	β_{b2}	φ
K1	4.2388e7	4.1699e7	4.3788e7	4.2689e7	4.3109e7
K2	4.2949e7	4.3870e7	4.3163e7	4.2370e7	4.1724e7
K3	4.1731e7	4.3021e7	4.1370e7	4.3489e7	4.3755e7
K4	4.4587e7	4.3065e7	4.3308e7	4.3107e7	4.3067e7
$\overline{K1}$	1.0597e7	1.0425e7	1.0947e7	1.0672e7	1.0777e7
$\overline{K2}$	1.0737e7	1.0968e7	1.0791e7	1.0593e7	1.0431e7
$\overline{K3}$	1.0433e7	1.0755e7	1.0342e7	1.0872e7	1.0939e7
$\overline{K4}$	1.1147e7	1.0766e7	1.0827e7	1.0777e7	1.0767e7
Range	0.0714e7	0.0543e7	0.0605e7	0.0279e7	0.0508e7
Sequencing	1	3	2	5	4

Displacement SN:

$$\eta_i = -10\log\frac{1}{n}\sum_{i=1}^{n} Y_i^2. \tag{6}$$

Stress SN:

$$\eta_j = -10\log\frac{1}{n}\sum_{j=1}^{n} Y_j^2. \tag{7}$$

Comprehensive SN:

$$\eta = 0.6\eta_i + 0.4\eta_j. \tag{8}$$

The results of SNR calculation are shown in Table 13.

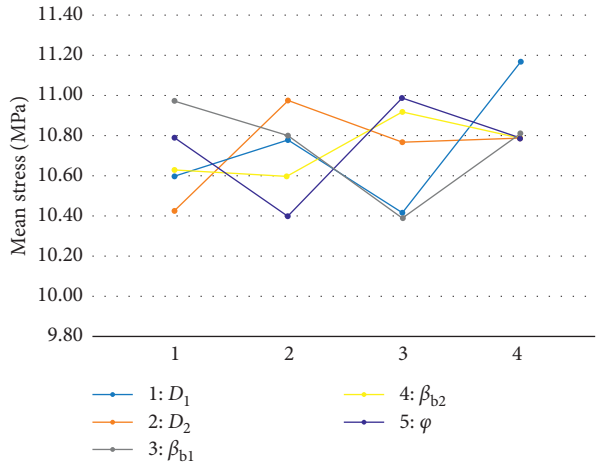

Figure 14: Influence trend of various parameters on stress.

Table 10: Comprehensive weighted score value table of orthogonal experimental results of the plastic-lined pump structure.

Sequence number	Displacement	Grade	Stress	Grade	Comprehensively weighted grading Y^*
1	0.0010517	86	9.4958e6	92	88.4
2	0.0010629	80	9.2606e6	98	87.2
3	0.0010706	78	9.5837e6	88	82
4	0.0010470	92	1.0391e7	84	88.8
5	0.0010151	100	1.0745e7	76	90.4
6	0.0010486	88	1.0914e7	72	81.6
7	0.0010565	84	1.0403e7	82	83.2
8	0.0011110	70	9.3839e6	96	80.4
9	0.0010288	98	9.1055e6	100	98.8
10	0.0010454	94	1.1593e7	70	84.4
11	0.0010586	82	9.5659e6	90	85.2
12	0.0010863	74	9.4928e6	94	82
13	0.0010448	96	1.0801e7	74	87.2
14	0.0010479	90	1.0677e7	80	86
15	0.0010845	76	1.0732e7	78	76.8
16	0.0010888	72	9.8617e6	86	77.6

Table 11: Controllable factors and their levels.

	Inlet diameter D_1 (mm)	Outlet diameter D_2 (mm)	Inlet angle β_{b1} (°)	Outlet angle β_{b2} (°)	Wrap angle φ (°)
1	72	252	18	20	100
2	74	254	22	24	105
3	76	256	26	28	110
4	78	258	30	32	115

According to the intuitive analysis in the above table, the signal-to-noise ratio of the test group 9 was the largest. $SN_{max} = -19.8206$; the corresponding process combination parameter was $A_3B_1C_3D_4E_2$.

4.10.2. Statistics of Internal Tables

(1) Find the sum of SN ratios (T):

$$T = \sum_{i=1}^{16} T_i. \tag{9}$$

Substitute the result to calculate $T = \sum_{i=1}^{16} T_i = -325.3347$.

(2) Find the sum of SN ratios was T_i, the average value of t_i, and the range R_i of each column under the horizontal conditions of each factor: $i = 1, 2, 3, 4$. The calculation results are shown in Table 14.

(3) Find the sum of the total fluctuation squares of SN ratio and S_T:

From the above calculation results, it can be seen that

$$\begin{aligned} T &= -325.3347, \\ \overline{y} &= \frac{T}{n} = -20.3342, \\ S_T &= \sum_{i=1}^{16} (y_i - \overline{y})^2, \\ S_T &= 0.749729444. \end{aligned} \tag{10}$$

Table 12: Inner table of orthogonal experiment.

	Inlet diameter D_1 (mm)	Outlet diameter D_2 (mm)	Inlet angle β_{b1} (°)	Outlet angle β_{b2} (°)	Wrap angle φ (°)
1	72	252	18°	20°	100°
2	72	254	22°	24°	105°
3	72	256	26°	28°	110°
4	72	258	30°	32°	115°
5	74	252	22°	28°	115°
6	74	254	18°	32°	110°
7	74	256	30°	20°	105°
8	74	258	26°	24°	100°
9	76	252	26°	32°	105°
10	76	254	18°	28°	100°
11	76	256	30°	24°	115°
12	76	258	22°	20°	110°
13	78	252	30°	24°	110°
14	78	254	26°	20°	115°
15	78	256	22°	32°	100°
16	78	258	18°	28°	105°

Table 13: Results of SNR calculation.

Sequence	A	B	C	D	E	SNR η_i	SNR η_j	Comprehensive SNR η
1	72	252	18°	20°	100°	59.56216	−139.5566	−20.0829
2	72	254	22°	24°	105°	59.47015	−139.3328	−20.0505
3	72	256	26°	28°	110°	59.40746	−139.6307	−20.2078
4	72	258	30°	32°	115°	59.60107	−140.3332	−20.3726
5	74	252	22°	28°	115°	59.8698	−140.6241	−20.3278
6	74	254	18°	32°	110°	59.5878	−140.7597	−20.5512
7	74	256	30°	20°	105°	59.5226	−140.3432	−20.4237
8	74	258	26°	24°	100°	59.08572	−139.4477	−20.3276
9	76	252	26°	32°	105°	59.75338	−139.1861	−19.8206
10	76	254	18°	28°	100°	59.61435	−141.2839	−20.7450
11	76	256	30°	24°	115°	59.50536	−139.6145	−20.1426
12	76	258	22°	20°	110°	59.28100	−139.5479	−20.2506
13	78	252	30°	24°	110°	59.619337	−140.6693	−20.4961
14	78	254	26°	20°	115°	59.593603	−140.5690	−20.4714
15	78	256	22°	32°	100°	59.295409	−140.6136	−20.6693
16	78	258	18°	28°	105°	59.261038	−139.8790	−20.3950

Table 14: T_i, t_i, and R_i of SN ratio at various factors.

	A	B	C	D	E
T_1	−80.7138	−80.7274	−81.7741	−81.2286	−81.8248
T_2	−81.6303	−81.8181	−81.2982	−81.0168	−80.6898
T_3	−80.9588	−81.4434	−80.8274	−81.6756	−81.5051
T_4	−82.0318	−81.3458	−81.4350	−81.4137	−81.3144
t_1	−20.17845	−20.18185	−20.44353	−20.30715	−20.4562
t_2	−20.40758	−20.45453	−20.32455	−20.2542	−20.17225
t_3	−20.23970	−20.36085	−20.20685	−20.4189	−20.37643
t_4	−20.50795	−20.33645	−20.35875	−20.35343	−20.32860
R	0.3295	0.272675	0.236675	0.16470	0.28975

(4) The sum of the squared fluctuations of SN ratio of each factor:

$$S_i = \frac{1}{4}\left(T_1^2 + T_2^2 + T_3^2 + T_4^2\right) - \frac{1}{16}T^2. \quad (11)$$

Substitute in the numerical value to get $S_1 = 0.2750$; $S_2 = 0.1536$; $S_3 = 0.11545352$; $S_4 = 0.058691812$; $S_5 = 0.146984112$; and $S_1 + S_2 + S_3 + S_4 + S_5 = 0.749729444$.

4.10.3. Analysis of Variance. Since there was no blank column in this experiment, that is, no error term, the minimum S4 was taken as the squared sum of error fluctuations, It can be obtained that $f_A = f_B = f_C = f_D = f_E = 4 - 1 = 3$. The analysis of variance is shown in Table 15.

From the perspective of SNR comparison, factor A has a significant impact on the quality fluctuation characteristics. It could be considered that factor A was a stabilizing factor and factors B, C, D, and E were adjustable factors. For the stabilizing factor, its level is taken as A_3, and the total displacement SNR of factors B, C, D and E is listed in Table 16.

Since the influence of factors B, C, D, and E on the quality fluctuation characteristics was not very significant, it can be considered to ignore the stress and simply adjust the parameters of B, C, D, and E to minimize the stress. As can be seen from the above table, the optimal process parameter was $B_1C_4D_4E_4$, considering only the stress. Finally, the optimized combination parameter was $A_3B_1C_3D_2E_2$, which was basically consistent with the optimal combination

Table 15: Variance analysis table.

	S	f	V	F
A	0.2750	3	0.091667	4.685492 (*)
B	0.1536	3	0.0512043	2.617060
C	0.11545352	3	0.038485	1.967115
D	0.058691812	3	0.0195639	1
E	0.146984112	3	0.048995	2.504338
(e)	(0.058691812)	(3)	(0.0195639)	
T	0.749729444	12		

Table 16: SN ratio response table of factors B, C, D, and E.

	B	C	D	E
1	238.8047	238.0253	237.9594	237.5576
2	238.2668	237.9173	237.6815	238.0081
3	237.7308	237.8402	238.1526	237.8956
4	237.2288	238.2484	238.2377	238.5698

parameter $A_3B_1C_3D_4E_2$ obtained by the intuitive method above.

4.11. Optimizing Model Validation. The accuracy of the optimization model was verified by thermo-solid coupling analysis of the optimized impeller structure parameter model. The thermo-solid coupling simulation results of the optimized model are shown in Figures 15 and 16. By comparing with the thermo-solid coupling simulation results before optimization, it can be seen that the total displacement and stress distribution after optimization were smaller than those before optimization. Figures 17 and 18 are, respectively, the total displacement and deformation diagram and stress distribution diagram before optimization.

In Taguchi algorithm, based on the above orthogonal experiment, the internal table of orthogonal experiment was designed and established to calculate the SNR of total displacement and stress distribution under various horizontal conditions, and its variance was calculated; by analyzing the calculated variance, the stability factor and adjustable factor could be obtained, then the adjustable factor could be optimized twice, and the final optimal process combination parameter can be obtained as $A_3B_1C_3D_2E_2$, When the inlet diameter D_1 was 76 mm, the outlet diameter D_2 was 252 mm, the inlet angle was 26°, the outlet angle was 24°, and the wrap angle was 115°, the total displacement, deformation, and stress of the pump were the minimum. Simulation results showed that the optimal combination was reasonable.

5. Performance Test of Lining Plastic Pump

5.1. Model Conversion. The principle of similitude conversion of plastic lining pump was to select a model which was equal to or similar to the designed pump speed to carry out similar conversion of its flow components [18]. Model pumps can be selected by referring to the design manual [3]: IS50-32-200: $Q_M = 12.5\ m^3/h$, $n_{SM} = 33$, $n_M = 2900$ rpm, $D_{1M} = 48$ mm, $D_{2M} = 198$ mm, $b_{2M} = 4$ mm, $b_{3M} = 12$ mm, and $Z_M = 6$. The structure parameters of the lining plastic pump optimized under fluid-thermal-structure interaction conditions were as follows: $Q_M = 25\ m^3/h$, $H_M = 80$m, $n_{SM} = 32.98$, $n_M = 2900$ rpm, $D_1 = 76$ mm, $D_{2M} = 252$ mm, $b_{2M} = 6.8$ mm, $b_{3M} = 42$ mm, and $Z_M = 6$.

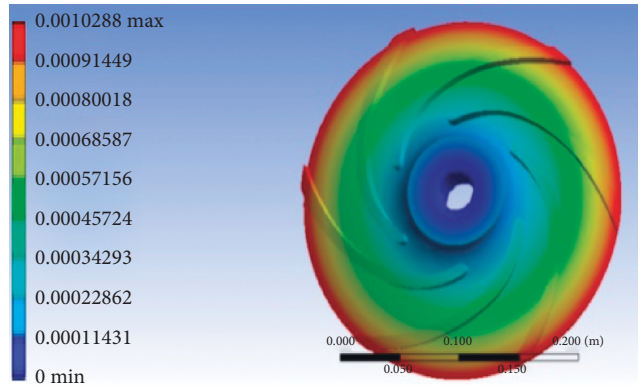

Figure 15: Total displacement and deformation after optimization.

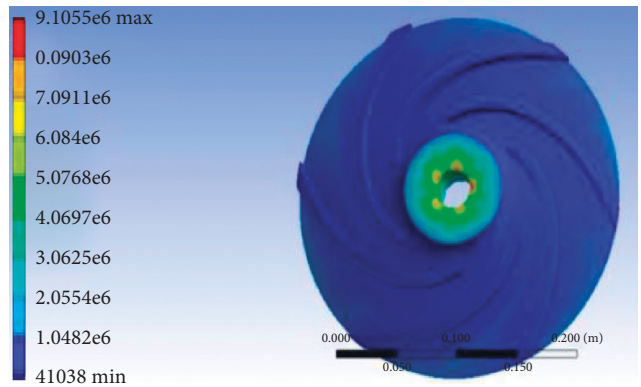

Figure 16: Stress distribution diagram after optimization.

5.1.1. Printing the Physical Impeller. The physical model was manufactured according to the similar converted liner pump structure parameters. Similar parameter combination was as follows: after the conversion, impeller inlet diameter D_1 was 60 mm, impeller outlet D_2 was 200 mm, inlet angle was 26°, outlet angle was 32°, and wrap angle was 105°. According to this set of parameters, three-dimensional modeling of the impeller structure of the lining plastic pump was conducted, as shown in Figure 19. The physical model is shown in Figure 20.

5.2. Performance Experiment. The similar model obtained by the similar conversion method was used for 3D printing, and the similar converted physical model was printed and then used in the external characteristic performance experiment [19, 20]. The experimental data collection platform of the lining plastic pump was equipped with the pump test system (electrical test method) V8.97 software specially used to collect the performance data onto the lining plastic pump. Data points of lift H and flow Q of each working point collected by the lining plastic pump under different flow conditions are included in Table 17.

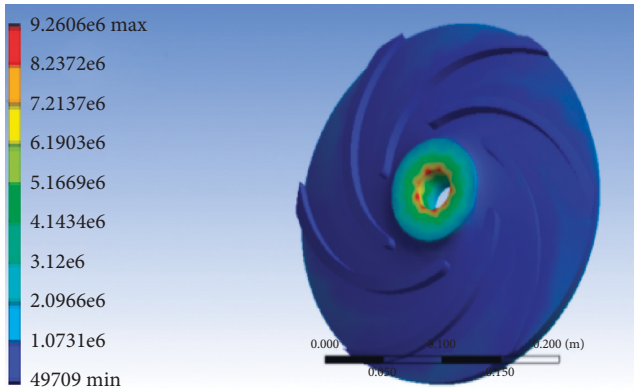

Figure 17: Total displacement and deformation before optimization.

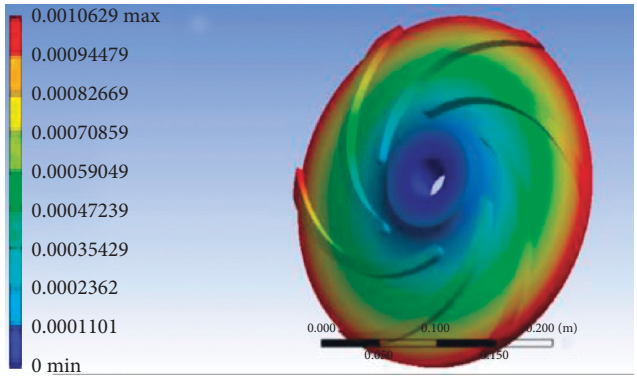

Figure 18: Stress distribution before optimization.

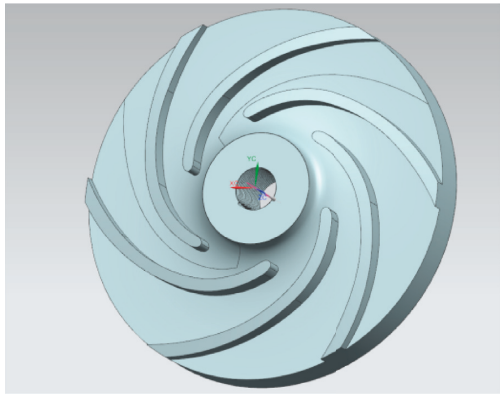

Figure 19: Three-dimensional diagram of lining pump.

It can be seen from Table 17 that, as the flow Q decreases, the head was gradually increased, and when the flow of the lining plastic pump was located in the $Q = 2.37\ m^3/h$, its head was about 12m, which was greatly different from the value of $H_M = 50$ m of the model pump used for similar conversion. The reasons for this deviation mainly included the following aspects:

(1) Excessive clearance: as the axial size of the inner cavity of the volute was relatively large, large clearance will be generated at the front end of the impeller when the impeller was installed inside the pump housing (Figure 21); the impeller front gap is too large, which causes the liquid backflow between the pump shell and the impeller, seriously affecting the hydraulic performance of the entire the lining plastic pump.

Figure 20: Picture of lining plastic pump.

(2) Cracks on the pump shell: the pipe at the outlet of the pump shell was a metal pipe. This metal pipe had certain stiffness, which led to the installation of it with the pump shell outlet face, as shown in Figure 22. Small cracks appear on the surface of the water outlet pipe of the pump shell when the water outlet pipe and the pipe fitting surface of the pump shell are installed, as shown in Figure 23. When the pump shell was filled with water, slight seepage water was found, the water in the whole pump chamber was dried, and glass glue was applied to the tiny crack of the pump shell. Although it does not impede the experiment, it will affect the pressure at the outlet of the pump, causing a decrease in the outlet pressure and a decrease in head of pump.

(3) Water accumulation at the outlet flange: due to the loose fitting between the outlet pipe and the pump casing, there was a wraping angle, and rubber gasket was added at the two joint surfaces, but the wraping angle of the joint has not been fully compensated. Afterwards, a certain thickness of glass glue was applied between the two bonding surfaces to make up the wrap angle gap. However, the high-speed rotation of the water from the pump shell through the impeller at the outlet had a certain pressure, so that it still has water accumulation in the outlet flange, and the water leakage occurs for a long time, as shown in Figure 24. Leakage at the outlet flange seriously affects the outlet pressure of the pump, resulting in a significant reduction in the lift.

Taking the minimum displacement and deformation of the impeller as the reference index, using the comprehensive weighted scoring method and the Taguchi algorithm to optimize the parameters of the thermal-solid coupling analysis of the lining plastic pump flow, the optimal combination parameters under the condition of the minimum

Table 17: Experimental table of performance of lining plastic pump.

Product model	Fluid density (kg/m^3): water	Export caliber (mm): 80						
Product number: 001	Fluid viscosity (cst): water	Surface distance (m): 0.0						
Manufacturer: Anhui Polytechnic University School of Mechanical and Automotive Engineering		Water temperature (°C): 11						
	Measurement set number					Switch to rated speed = 1450 (r/min)		
Serial number	Import pressure (kPa)	Export pressure (kPa)	Traffic (m^3/h)	Rotation speed (r/min)	Input power (W)	Traffic (m^3/h)	Head (m)	Shaft power (W)
1	7.79	21.62	33.85	1448.30	1363.97	67.78	6.08	8292.97
2	8.23	24.64	30.06	1447.93	1398.90	60.21	7.05	8560.39
3	8.52	26.87	27.05	1447.65	1431.84	54.19	7.78	8806.19
4	8.80	28.90	23.99	1461.60	1439.54	47.60	8.28	8711.76
5	9.05	30.92	20.93	1477.68	1490.61	41.08	8.74	8895.00
6	9.26	32.74	18.08	1447.91	1477.37	36.21	9.73	9158.49
7	9.45	34.71	14.98	1447.11	1472.91	30.02	10.43	9127.00
8	9.60	35.42	12.06	1447.97	1473.81	24.15	10.61	9131.15
9	9.74	36.87	8.93	1447.68	1433.57	17.89	11.13	8829.37
10	9.83	38.51	6.09	1447.68	1388.37	12.20	11.75	8488.16
11	9.86	39.08	4.01	1448.56	1297.83	8.03	11.95	7794.08
12	9.88	39.21	2.37	1448.92	1264.31	4.74	11.98	7539.48

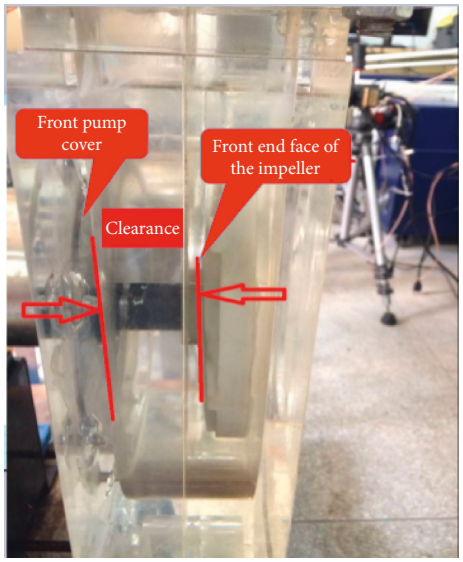

Figure 21: Schematic diagram of the impeller clearance of the lining plastic pump.

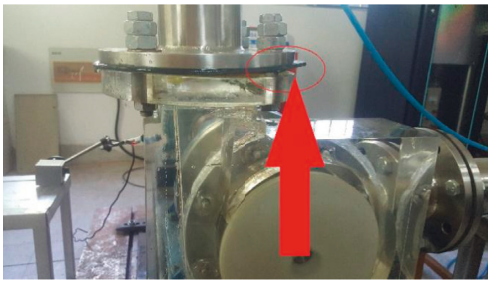

(a)

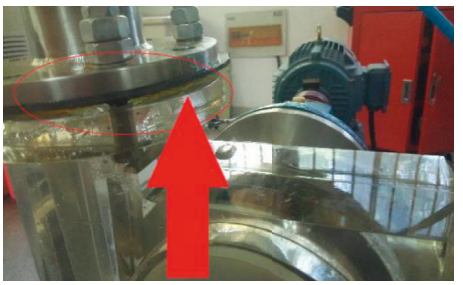

(b)

Figure 22: Warping position of water outlet pipe and pump shell joint.

displacement and stress were obtained as $A_3B_1C_3D_2E_2$, that is, when the inlet diameter D_1 was 76 mm, the outlet diameter D_2 was 252 mm, the inlet angle was 26°, the outlet angle was 24°, and the wrap angle was 115°, and the total displacement, deformation, and stress of the pump were minimal.

6. Conclusion

(1) In this paper, the orthogonal experimental table of $L^{16}(4^5)$ was designed and the orthogonal experiment was carried out; it can be concluded that the influence of each factor on the efficiency of the lining plastic centrifugal pump was from large to small: impeller outlet diameter D_2, wrap angle φ, inlet diameter D_1, inlet angle β_{b1}, and outlet angle β_{b2}, and the influence of various factors on cavitation of the centrifugal pump is in the following order: inlet angle β_{b1}, wrap angle φ, impeller outlet diameter D_2, outlet angle β_{b2}, and inlet diameter D_1;

(2) Under the condition of fluid-solid coupling, when the total displacement was taken as the optimization index, the optimal horizontal combination was the inlet diameter D_1 is 76 mm, the outlet diameter D_2 was 252 mm, the inlet angle was 26°, the outlet angle was 32°, and the wrap angle was 115°; the total displacement can be obtained to be the minimum,

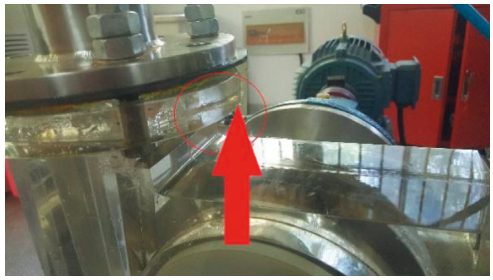

Figure 23: Location of pump shell crack.

(a)

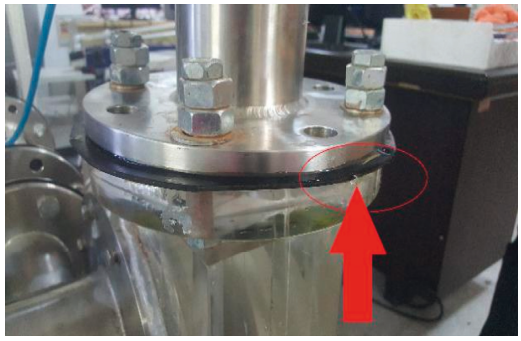

(b)

Figure 24: Water location of exit flange.

indicating that the plastic pump under this parameter had the minimum deformation; when the stress was taken as the optimization index, the optimal combination is that the inlet diameter D_1 was 76 mm, the outlet diameter D_2 was 252 mm, the inlet angle was 26°, the outlet angle was 24°, and the wrap angle was 105°; the minimum stress can be obtained, which indicated that the plastic pump under this parameter had the minimum stress.

(3) Taking the minimum displacement and deformation of the impeller as the optimization index, using Taguchi algorithm to optimize the parameters of the flow thermo-solid coupling analysis of the lining plastic pump flow, the optimal combination parameters under the condition of the minimum displacement and stress were obtained: when the inlet diameter D_1 was 76 mm, the outlet diameter D_2 was 252 mm, the inlet angle was 26°, the outlet angle was 24°, and the wrap angle was 115°, the total displacement deformation and stress of plastic pump lining were minimum.

Data Availability

We guarantee that the data in this article are true and reliable, and the data used to support the findings of this study are available from the corresponding author upon request.

Conflicts of Interest

The authors declare that they have no conflicts of interest.

Acknowledgments

This article belongs to the major projects of the "Natural Science Foundation of Anhui Province Education Department" (KJ2016SD05 and KJ2017ZD12).

References

[1] Zhu Hongjun, *ANSYS 14.5 Practical Guide to Thermal Fluid-Solid Coupling*, People's Posts and Telecommunications press, Beijing, China, 2014.

[2] M. Duan, H. Yu, and X. Ge, "Three-dimensional flow field analysis of centrifugal pumps based on CFD," *Journal of Liaoning University of Technology*, vol. 35, no. 6, pp. 392–395, 2015.

[3] Y. Li, W. Dong, Z. He, Y. Huang, and X. Jiang, "Flow instability of a centrifugal pump determined using the energy gradient method," *Journal of Thermal Science*, vol. 24, no. 1, pp. 44–48, 2015.

[4] E. C. Bacharoudis, A. E. Filios, M. D. Mentzos, and D. P. Margaris, "Parametric study of a centrifugal pump impeller by varying the outlet blade angle," *Open Mechanical Engineering Journal*, vol. 2, no. 5, pp. 75–83, 2008.

[5] R. Zhang, J. Yang, and R. Li, "Parametric design of centrifugal pump impeller," *Journal of Drainage and Irrigation Mechanical Engineering*, vol. 27, no. 5, pp. 310–313, 2009.

[6] M. Li, J. Kou, D. Lin et al., *Basic Theory and Application of Genetic Algorithm*, Science Press, Beijing, China, 2002.

[7] S. Zhou and J. Liao, "Study on the working characteristics of fracturing pump head based on thermo-solid coupling," *Science and Technology and Engineering*, vol. 15, no. 25, pp. 38–43, 2015.

[8] A. Lucius and G. Brenner, "Unsteady CFD simulations of a pump in part load conditions using scale-adaptive simulation," *International Journal of Heat and Fluid Flow*, vol. 31, no. 6, pp. 1113–1118, 2010.

[9] D. Bonaiuti, M. Zangeneh, R. Aartojarvi et al., "Parametric design of a waterjet pump by means of inverse design, CFD calculations and experimental analyses," *Journal of Fluids Engineering*, vol. 132, no. 3, pp. 0311041–0311045, 2010.

[10] B. Zhao, T. Sun, C. Zhou, and Y. Wang, "Optimization design of centrifugal pump impeller based on CFD technology," *Petrochemical Equipment Technology*, vol. 28, no. 6, pp. 43–45, 2007.

[11] R. W. Westra, L. Broersma, A. K. Van et al., "PIV measurements and CFD computations of secondary flow in a centrifugal pump impeller," *Journal of Fluids Engineering*, vol. 132, no. 6, pp. 0611041–0611048, 2010.

[12] X. Wang and L. Zhang, "Design of built-in permanent magnet synchronous click multi-objective optimization based on

taguchi algorithm," *Microelectromechanical*, vol. 49, no. 5, pp. 1–5, 2016.

[13] W. Xiaoling and L. Zhao, "Determination of comprehensive weighted scoring value of multi-index experimental design," *Journal of Hebei Architecture and Technology*, vol. 20, no. 4, pp. 68–72, 2003.

[14] L. Wan, W. Song, J. Yu, L. Xu, and J. Chen, "Effects of blade envelope Angle on hydraulic performance of centrifugal pump with high specific speed," *Renmin Yangtze River*, vol. 49, no. 15, pp. 96–100, 2008.

[15] H. Schmucker, F. Flemming, and S. Coulson, "Two-way coupled fluid structure interaction simulation of a propeller turbine," in *Proceedings of 25th IAHR on Hydraulic Machinery and Systems*, p. 110, Timisoara, Romania, December 2010.

[16] Y. Wang, *Effects of Blade Envelope Angle and Outlet Angle on Impeller Performance*, Lanzhou University of Technology, Lanzhou, China, 2017.

[17] H. CAI and C. Yun, "Optimization of injection molding process based on regression orthogonal design and comprehensive weighted scoring," *Plastics Industry*, vol. 46, no. 9, pp. 67–71, 2008.

[18] W. Ju and Z. Li, "Experimental analysis and performance prediction of centrifugal pump with medium specific speed," *China Rural Water Conservancy and Hydropower*, vol. 07, pp. 99–102, 2016.

[19] E Galenne, I Pierre-Danos, N Brunetiere, and B. Tournerie, "Influence of secondary Orings on hydrostatic mechanical seals in PWR reactor coolant pumps," in *Proceedings of Advanced Topics and Technical Solutions in Dynamic Sealing Workshop*, pp. 45–57, Poitiers, France, October 2005.

[20] G. Merckling, "Long-term creep rupture strength assessment: development of the european collaborative creep committee post-assessment tests," *Pressure Vesselsand Piping*, vol. 2, no. 13, pp. 2–12, 2008.